THE JOURNAL OF BIOLOGICAL CHEMISTRY VOL. 287, NO. 37, pp. 31371–31381, September 7, 2012

Disruption of the Bacteriophage T4 Mre11 Dimer Interface Reveals a Two-state Mechanism for Exonuclease Activity*[S]

Received for publication, June 15, 2012, and in revised form, July 10, 2012 Published, JBC Papers in Press, July 13, 2012, DOI 10.1074/jbc.M112.392316

Dustin W. Albrecht, Timothy J. Herdendorf, and Scott W. Nelson[1]

From the Department of Biochemistry, Biophysics, and Molecular Biology, Iowa State University, Ames, Iowa 50011

Background: The Mre11 dimer interface may be dynamic, responding to ATP and/or DNA.
Results: A mutation in the Mre11 dimer interface increases the nuclease initiation rate but decreases the translocation rate and lowers processivity.
Conclusion: Mre11 cycles between at least two states during its catalytic cycle.
Significance: The first state is for assembly/initiation and the second state is for translocation.

The Mre11-Rad50 (MR) complex is a central player in DNA repair and is implicated in the processing of DNA ends caused by double strand breaks. Recent crystal structures of the MR complex suggest that several conformational rearrangements occur during its ATP hydrolysis cycle. A comparison of the Mre11 dimer interface from these structures suggests that the interface is dynamic in nature and may adopt several different arrangements. To probe the functional significance of the Mre11 dimer interface, we have generated and characterized a dimer disruption Mre11 mutant (L101D-Mre11). Although L101D-Mre11 binds to Rad50 and dsDNA with affinity comparable with the wild-type enzyme, it does not activate the ATP hydrolysis activity of Rad50, suggesting that the allosteric communication between Mre11 and Rad50 has been interrupted. Additionally, the dsDNA exonuclease activity of the L101D-MR complex has been reduced by 10-fold under conditions where processive exonuclease activity is required. However, we unexpectedly found that under steady state conditions, the nuclease activity of the L101D-MR complex is significantly greater than that of the wild-type complex. Based on steady state and single-turnover nuclease assays, we have assigned the rate-determining step of the steady state nuclease reaction to be the productive assembly of the complex at the dsDNA end. Together, our data suggest that the Mre11 dimer interface adopts at least two different states during the exonuclease reaction.

Double strand breaks (DSB)[2] are among the most harmful forms of DNA damage, and they may lead to deletions, duplications, or cell death if they go unrepaired (1). DSBs are common and can result from both internal and external causes. External causes include ultraviolet radiation, ionizing radiation, and genotoxic chemicals. Internal causes include reactive oxygen species and protein complexes that interfere with replication fork progression. DSBs are also deliberately formed during the development of antibodies through VDJ recombination (2).

The three pathways for repairing DSBs in eukaryotic cells have been described in the literature: homologous recombination, nonhomologous end-joining, and microhomology-mediated end-joining (3). Mre11 and Rad50 form a heterotetrameric complex ($Mre11_2$-$Rad50_2$, referred to as the MR complex hereafter) that is involved in all three of the above mentioned DSB repair pathways (3, 4). The role of the MR complex is best understood in homologous recombination, which involves several steps and requires multiple proteins (5). The MR complex is involved in the initial step of homologous recombination, which is the resection of the 5′ strand of the DSB to create 3′ single-stranded DNA. The role of the MR complex in this process has been recently elucidated using the *Saccharomyces cerevisiae* model system (6–8). Resection is a two-step process in eukaryotes with the MR complex being essential for the first step. In the first step of *S. cerevisiae* cells, the MR complex works along with Xrs2 and Sae2 to remove 50–100 nucleotides (nts) from the 5′ end of the DSB (6). In the second step, the intermediates created by the MR complex are further resected (>500 nts) by Sgs1/Top3/RmiI and RPA or ExoI and RPA. Upon completion of DSB resection, Rad51 promotes strand invasion of the ssDNA into a region of homologous DNA and creates a D-loop that is used as a primer for DNA synthesis (9). Upon completion of DNA synthesis, either the extended strand is liberated from the template by a DNA helicase or the Holliday junction is resolved by a DNA nuclease and ligase (10).

The MR complex is present in eukaryotes, archaea, prokaryotes, and some bacteriophage biological systems (4). Although the MR complex homologs from eukaryotes, archaea, and bacteriophage participate in DSB resection, the prokaryotic MR homolog, the SbcCD complex, does not seem to be involved in DSB resection, instead prokaryotic resection is carried out by the RecBCD helicase-nuclease complex (11). The T4 bacteriophage homologs of the MR complex (gp46/gp47) are required for *in vivo* homologous recombination and DSB repair, and T4 bacteriophage has been used as a model system

* This work was supported by Carver Trust Young Investigator Grant 10-3603 (to S. W. N.), Iowa State University institutional support (to S. W. N.), and National Science Foundation Grant MCB-1121693 (to S. W. N.).
[S] This article contains supplemental Figs. S1–S3.
[1] To whom correspondence should be addressed. Tel.: 515-294-3434; Fax: 515-294-0453; E-mail: swn@iastate.edu.
[2] The abbreviations used are: DSB, double strand break; gp46, T4 gene product 46; gp47, T4 gene product 47; 2-AP, 2-aminopurine deoxyribonucleotide; MR, Mre11/Rad50; NBD, nucleotide binding domain; ssDNA, single-stranded DNA; ABC, ATP-binding cassette; MR-DNA, Mre11-Rad50-DNA complex; nt, nucleotide; RPA, replication protein A; AUC, analytical ultracentrifugation.

for the investigation of nucleic acid enzymes for many years (12–14).

Rad50 belongs to the structural maintenance of chromosome protein family, which is a subset of the ATP-binding cassette (ABC) protein superfamily (15, 16). The ABC superfamily of proteins is broadly distributed and contains a well conserved dimeric nucleotide binding domain (NBD) that binds and hydrolyzes ATP at its dimeric interface (17). The energy obtained from ATP hydrolysis is used by ABC proteins to promote a variety of biological functions (17). T4 Rad50 (gp46) is an inefficient ATPase (k_{cat} of 0.15 s^{-1}), but it becomes much more active (k_{cat} of 3.2 s^{-1}) upon the addition of Mre11 and double-stranded DNA (dsDNA) (18). Although it does not affect the initial rate of nucleotide removal, ATP hydrolysis increases the rate of repetitive nucleotide removal leading to the hypothesis that ATP hydrolysis is involved in MR complex translocation along the DNA substrate (18, 19).

Mre11 is a member of the Ser/Thr protein phosphatase superfamily, which requires divalent cations for their catalytic activity (20). *In vitro* assays have shown that T4 Mre11 (gp47) contains the nuclease subunit of the MR complex and has single-stranded DNA (ssDNA) endonuclease, dsDNA exonuclease, and a probable end-dependent dsDNA endonuclease activity (18). Knock-out of Mre11 in *S. cerevisiae* causes only mild effects but has a much more profound impact in humans (21, 22). Mre11 deficiency in humans can lead to ataxia telangiectasia-like disorder, which causes ionizing radiation sensitivity and cerebellar dysfunction (23).

Several recent crystal structures have greatly clarified the architecture of the heterotetrameric MR complex. A combination of small angle x-ray scattering and x-ray crystallography using full-length Mre11 and Rad50 with the majority of its coiled coil and all of the zinc-hook removed revealed that the M_2R_2 heterotetramer can exist in at least two different conformations, termed open and closed (24–28). In the open conformation, the nucleotide binding domains (NBDs) of Rad50 are far away from each other with Mre11 acting as a bridge holding the heterotetramer together (24). In the presence of ATP or an ATP analog, the Rad50 nucleotide binding domains come together and form the classic sandwich dimer that has been observed in many ABC proteins. A surprising feature of these new structures has been the relative position of Mre11 with respect to the coiled-coil domain of Rad50. Instead of being placed between the coiled coils of Rad50 as it has been traditionally depicted in schematic models, Mre11 embraces Rad50 on the surface of Rad50 opposing the coiled-coil domain (27, 28). As a consequence of this arrangement, the nuclease active sites of Mre11 are somewhat protected by Rad50 so that it appears difficult for anything larger than ssDNA to approach the Mre11 active site. Hopfner and co-workers (27) have identified at least four separate Mre11-Rad50 interfaces that contribute to stabilizing the MR complex heterotetramer. The most extensive interface is formed through a C-terminal helix-loop-helix of Mre11 that interacts with the base of the coiled-coil domain of Rad50. Also interacting with the base of the coiled coil of Rad50 is the linker domain that separates the helix-loop-helix and cap domains of Mre11. The remaining interfaces are formed through interactions between the Mre11 cap and phosphoesterase domains and the nucleotide binding domain of Rad50. Any or all of these domains may be involved in allosteric signal transmission between Mre11 and Rad50. Besides the four heterosubunit interfaces, there are three additional homosubunit interfaces, two from the Rad50 dimer and one from the Mre11 dimer. The most extensive homosubunit interface is that of the NBD of Rad50, which is typical of all ABC proteins and has been readily observed in many x-ray crystal structures (15). The second Rad50-Rad50 interface is the zinc-hook, which is found at the apex of the coiled-coil domain (29). This interface is defined by a shared Zn^{2+}-binding site that is formed through a tetrathiolate linkage where each coiled coil provides two cysteine residues. Although this type of binding site generally binds Zn^{2+} with extremely high affinity and is therefore thought to be extremely stable, atomic force microscopy experiments suggest that the Rad50 zinc-hook domain is dynamic and able to respond to DNA binding by Rad50 (30). The Mre11-Mre11 homodimeric interface is relatively small, made up of a four-helix bundle with two helices being provided by each subunit (Figs. 1 and 2*A*). The interaction between these helices is largely hydrophobic with the exception of two salt bridges. X-ray crystal structures and protein cross-linking indicate that the Mre11 dimeric interface undergoes small conformation rearrangements upon ATP binding by Rad50 (24, 27).

To explore the significance of the Mre11 dimeric interface, we utilized site-directed mutagenesis on T4 Mre11. A hydrophobic residue (Leu^{101}) located in the Mre11 dimeric interface was chosen and mutated. In an effort to determine the significance of the dimer interface, we investigated the effects of the mutation on the MR complex in terms of Rad50 and DNA affinity, activation of Rad50 ATP hydrolysis activity, and nuclease activity. Our assays show that disruption of the Mre11 dimeric interface has no effect on the affinity of Mre11 for Rad50. Also, the disrupted dimeric interface appears to have little effect on MR complex DNA binding and ssDNA endonuclease activity. However, the disruption has profound effects on the ATPase activity of Rad50 and the exonuclease activity of Mre11 in both steady state and pre-steady state assays.

EXPERIMENTAL PROCEDURES

Mutagenesis, Protein Expression, and Purification—The L101D-Mre11 mutant was constructed using the Stratagene QuikChange site-directed mutagenesis protocol. The presence of the mutation and the integrity of the entire open reading frame were verified using DNA sequencing. Bacterial expression and purification of the L101D-Mre11, wild-type Mre11 (WT-Mre11), and Rad50 proteins were carried out as described previously (18, 31).

Circular Dichroism (CD) Spectroscopy—CD studies on WT- and L101D-Mre11 were performed at 22 °C on a Jasco J710 CD spectrometer in a 1-cm cell using a protein concentration of ~0.25 mg/ml. The buffer used was 10 mM Tris-HCl, 200 mM NaCl, pH 7.6. Spectra were collected from 200 to 260 nm in increments of 0.2 nm. Each spectrum was blank-corrected, and L101D-Mre11 was normalized to the ellipticity of the WT protein at 210 nm to correct for differences in protein concentration.

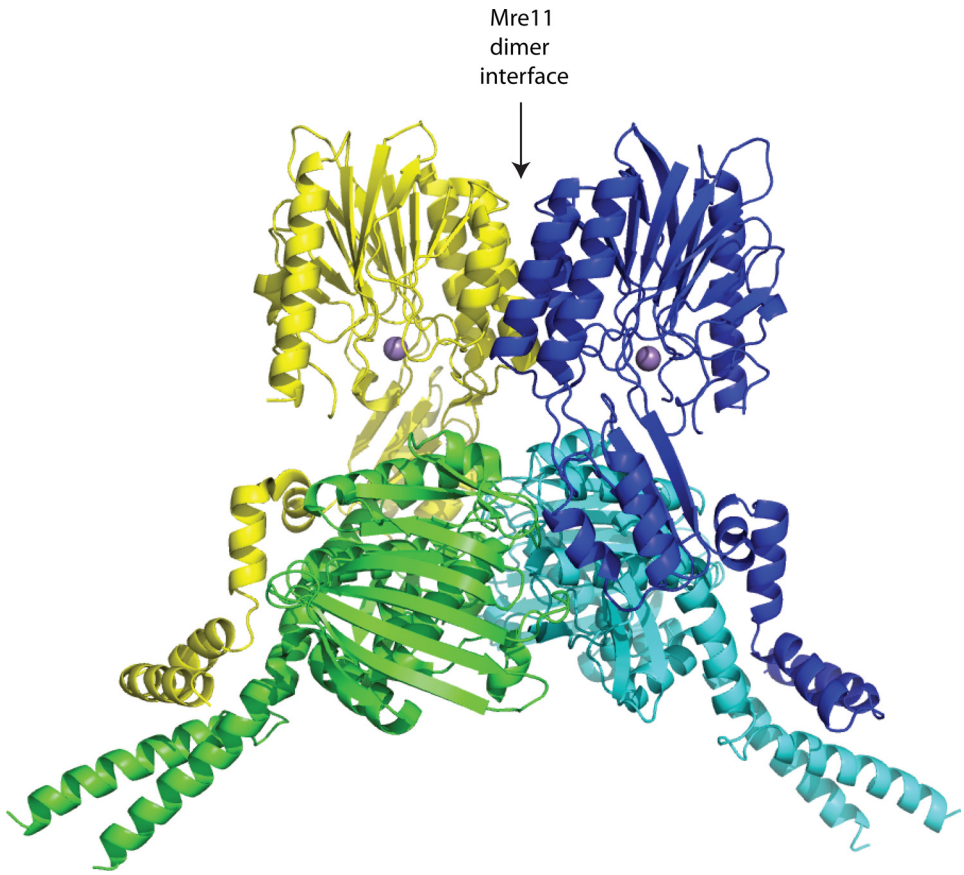

FIGURE 1. ***T. maritima*** **MR complex heterotetramer with truncated Rad50 coiled-coil domains.** The *ribbon* structure is based on Protein Data Bank code 3THO (25). The Rad50 subunits are colored *cyan* and *green*, and the Mre11 subunits are colored *blue* and *yellow*. The Mre11 dimer interface is indicated. Two molecules of ATP bind at the Rad50 interface, and the Mre11 nuclease active site is indicated by the *purple spheres* representing the active site Mn^{2+} ions.

ATP Hydrolysis Assays—Determinations of K_m, k_{cat}, and level of DNA activation were performed as described previously (18).

Competition by L101D-Mre11 with WT-Mre11 for Rad50—The relative affinity of the L101D-Mre11 mutant for Rad50 was determined using a coupled ATPase assay (32). All assays were done at 30 °C. The reaction was performed in a buffer containing 50 mM Tris-HCl, 50 mM KCl, 5 mM $MgCl_2$, 0.1 mg/ml BSA (referred to hereafter as "standard buffer") with 1 mM ATP, 1 μM DNA, 300 μM NADH, 2 mM phosphoenolpyruvate, 6 units/ml pyruvate kinase, and 10 units/ml lactate dehydrogenase at pH 7.6 in a volume of 125 μl. The sequences of the oligonucleotides used to create the DNA substrate were as follows: ds50-F, 5′-CTCTTGGTGATTATGATGGTTGCAATACATTTAATTTCATTATCAATAAG-3′, and ds50-R, 5′-CTTATTGATAATGAAATTAAATGTATTGCAACCATCATAATCACCAAGAG-3′. The oligonucleotides were dissolved in sterile water, quantitated by measuring the absorbance at 260 nm mixed in equal molar ratios, annealed by heating to 80 °C for 5 min, and slowly cooled to room temperature. In each assay, WT-Mre11 and Rad50 each had a concentration of 0.1 μM, whereas the L101D-Mre11 concentration had values of 0, 0.05, 0.1, 0.2, 0.4, 0.7, and 1.0 μM in each respective assay. ATP hydrolysis was assayed spectrophotometrically on a Varian Cary 50 UV-visible spectrophotometer by monitoring absorbance at 340 nm.

Nuclease Assays—The ssDNA endonuclease activity was monitored using single strand circular M13 DNA as a substrate (1 μg per lane). The reactions were carried out in standard buffer with 0.3 mM $MnCl_2$. Mre11 and Rad50 concentrations were held at 0.3 μM. At the indicated time points, 10 μl of reaction was removed and quenched with EDTA. Each time point was then run out on a 1% TAE-agarose gel containing ethidium bromide and visualized using UV light.

The steady state product profile of the MR complex was visualized using denaturing PAGE. All assays were done at 30 °C in standard buffer with 0.3 mM $MnCl_2$ in the presence of 1.3 μM hexachlorofluorescein-labeled DNA substrate. The hexachlorofluorescein label was attached to the 5′ end of the ds50-F primer and a phosphorothioate linkage was introduced between the 1st and 2nd nucleotides of the ds50-R substrate (relative to the 3′ end). The phosphorothioate linkage prevented Mre11 from excising nucleotides from the unlabeled DNA strand. The Mre11 and Rad50 concentrations varied and are denoted in each individual figure legend. Reactions that used an ATP regeneration system contained 1 mM ATP, 7 mM phosphocreatine, and 2 units of creatine kinase. The reactions were started by addition of the DNA substrate (containing ATP and $MnCl_2$) to an equal volume of the protein solution. At times 0, 5, 10, 15, 20, 30, 40, 50, 60, 70, 80, 90, 100, 110, and 120 min, a 12-μl aliquot was removed and quenched with an equal volume of quench buffer containing 50% formamide and 100 mM

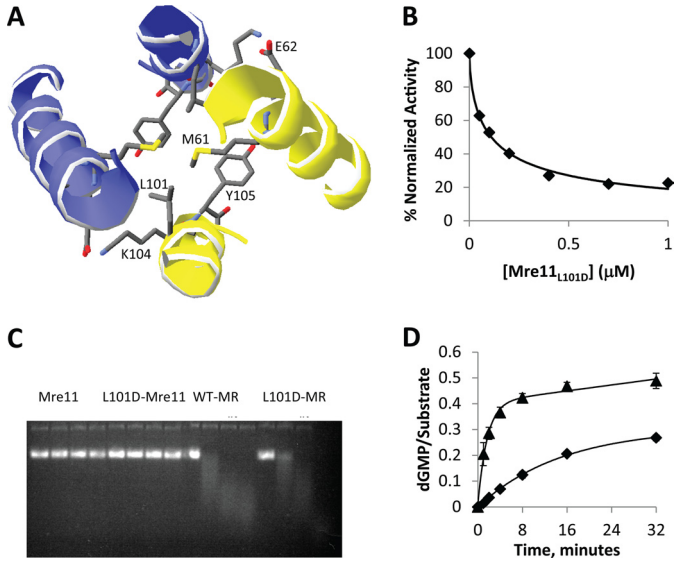

FIGURE 2. *A,* close-up view of the modeled T4 Mre11 dimer interface. The homology model was generated using the Swiss Model server (33) and based on the structure of the dimeric Mre11 from *P. furiosus*, Protein Data Bank code 3DSC (34). *B,* competition assay for Rad50. Each spectrophotometric ATPase assay consisted of the standard buffer with 0.1 μM WT-Mre11, L101D-Mre11 at the concentration indicated, 0.1 μM Rad50, 1 mM ATP, and 1.0 μM 50-bp dsDNA. *C,* ssDNA endonuclease activity assays. The four time points for each indicated condition are 0, 8, 16, and 32 min. *D,* blunt-ended dsDNA exonuclease activity assays. Assays were performed in standard buffer with 0.3 mM $MnCl_2$ at 30 °C. ATP concentrations of 0.25 and 0.185 mM were used for WT (*closed triangles*) and L101D (*closed squares*), respectively. Each assay consisted of 1 μM Rad50, 1.25 μM Mre11, and 5 nM DNA substrate. Time points were 0, 1, 2, 4, 8, 16, and 32 min. The *solid lines* are single-exponential fits to the data points, as described under "Experimental Procedures."

EDTA. The zero time point was taken prior to the initiation of the reaction by sequentially adding an aliquot of the protein solution and an aliquot of the DNA solution to the quench buffer. Reaction products were resolved with 16% denaturing PAGE containing 7.5 M urea in 1× TBE buffer. Gels were run for 3–3.5 h at a constant power of 60 watts. The gel was visualized on a Typhoon PhosphorImager using a 532 nm laser and a 555 nm bandpass filter and analyzed using the ImageJ software (National Institutes of Health).

The pre-steady state exonuclease assays were performed as described for the steady state assays with some exceptions. The DNA substrate was identical, except that a biotin group was attached to the 3′ end of the ds50-R DNA strand. The reactions included a 2-fold molar excess of streptavidin (tetramer) relative to DNA concentration to completely block the nuclease activity of Mre11 on the unlabeled DNA strand under high enzyme concentrations. The concentrations of DNA, Rad50, and Mre11 were 100 nM, 3 μM, and 3.15 μM, respectively. ATP concentrations used were five times the $K_{m,\,ATP}$ for each protein, and no ATP regeneration system was used. Time points for the assays were 0, 3, 5, 7, 10, 15, 20, 25, 30, 40, 50, 60, 80, 100, and 120 s.

The uniformly labeled 1.96-kb dsDNA used in the exonuclease reaction shown in Fig. 2*D* was prepared by performing a 100-μl PCR in Long Amp polymerase buffer using 5 units of Long Amp polymerase, 30 μCi of [α-^{32}P]dGTP, 0.25 mM cold dNTP mix, 1 μM T7 promoter primer, 1 μM T7 terminator primer, and 50 ng of the gp46-pET28a vector. The labeled PCR product was purified using the Qiagen PCR purification protocol. Three more PCRs were set up with the same conditions but lacking the [α-^{32}P]dGTP. They were subject to the same PCR cycle and purification protocols and quantitated using their A_{260} values. The three values were averaged and that value was used for the [α-^{32}P]dGTP-labeled product. The exonuclease reaction was performed in the standard buffer with 0.3 mM $MnCl_2$, 7 mM phosphocreatine, and 2 units/20 μl of creatine kinase at pH 7.6. Assays were performed at 30 °C and with 5 nM uniformly [α-^{32}P]dGTP-labeled 1.96-kb dsDNA. The ATP concentration was kept at five times the $K_{m,\,ATP}$ for each protein. Mre11 and Rad50 were at concentrations of 1.25 and 1.0 μM, respectively. The assays were started by addition of the DNA substrate to the protein solution. The assays were quenched by adding 2 μl of the assay to an equal volume of 250 mM EDTA. Time points of 0, 1, 2, 4, 8, 16, and 32 min were taken for both the WT- and L101D-MR complex. The zero time point was taken prior to the initiation of the reaction by sequentially adding an aliquot of the protein solution and an aliquot of the DNA solution to the quench buffer. The reactions were analyzed by spotting 2 μl onto Baker-flex cellulose PEI-F TLC plates and developed in 300 mM KP_i, pH 7.0. The TLC plates were dried and then exposed for 2 h to a PhosphorImager plate. After exposure, the plate was visualized on a Typhoon Phosphorimager and analyzed on the ImageJ software.

2-Aminopurine Assays—Nuclease activity was also probed spectrofluorometrically using DNA substrates with a fluorescent 2-aminopurine deoxyribonucleotide (2-AP) at either the 1st, 2nd, 5th, 9th, 12th, 17th, or 22nd position relative to the 3′ end of the substrate. The assays were performed in the standard buffer with 0.3 mM $MnCl_2$ and 1.3 μM DNA substrate. In assays containing ATP, the ATP concentration was five times the $K_{m,\,ATP}$ for each protein. Steady state exonuclease assays were performed at 30 °C, pH 7.6, in a volume of 300 μl. The concentration of the MR complex was held at 400 nM. An MR concentration of 100 nM was used in the assays probing the 1st and 2nd positions in the presence of ATP. An MR concentration of 50 nM was used in the L101D-MR complex assay probing the 1st position in the absence of ATP. Mre11 was always held in slight excess over Rad50 (1.05:1 ratio, Mre11/Rad50). The 2-AP was excited at a wavelength of 310 nm, and the increase in fluorescence was monitored at 375 nm on a Varian Cary Eclipse spectrofluorometer. Pre-steady state assays were performed using a Biologic SFM-400 stopped flow apparatus held at 30 °C in the standard assay buffer with 0.3 mM $MnCl_2$. In assays containing the WT-MR complex, the ATP, DNA, and protein concentrations were 1 mM, 200 nM, and 3 μM, respectively. In assays containing the L101D-MR complex, the ATP, DNA, and protein concentrations were 1 mM, 200 nM, and 2 μM, respectively. The nucleotide, DNA, and protein were held in separate syringes and simultaneously injected into the flow cell at time 0.

DNA Binding Assays—The DNA binding affinity of the MR complex was determined using a fluorescence polarization assay carried out with a Synergy 2 Multi-Mode microplate reader. All assays were done at ambient temperature in the standard buffer with 10 nM hexachlorofluorescein-labeled DNA substrate. Mre11 and Rad50 concentrations used were 12 μM followed by a series of 10 2-fold serial dilutions and a zero

TABLE 1

Steady state ATPase kinetic constants for WT and L101D MR-DNA complexes

Fluorometric assays were performed in 50 mM Tris-HCl, 50 mM KCl, 0.1 mg/ml BSA, pH 7.6, in the presence of 5 mM $MgCl_2$ at 30 °C. Values were determined by fitting data to a Hill equation. Errors represent the standard error of the fit.

Protein	K_m	k_{cat}	DNA activation[a]	n
	μM	s^{-1}		
Rad50[b]	16 ± 0.8	0.146 ± 0.003	NA[c]	1.4 ± 0.1
Rad50/Mre11[b]	42 ± 1	0.226 ± 0.006	NA	1.5 ± 0.1
Rad50/$Mre11_{L101D}$	50 ± 1	0.101 ± 0.002	NA	2.2 ± 0.2
Rad50/Mre11[b]	49 ± 2	3.2 ± 0.1	22	2.4 ± 0.2
Rad50/$Mre11_{L101D}$	37 ± 1	0.32 ± 0.01	2.2	2.5 ± 0.4

[a] Fold increase in k_{cat} between MR-DNA and Rad50 is shown.
[b] Values are from Ref. 18.
[c] NA means not applicable.

protein condition. In the MR complex assays, Mre11 was always held in slight excess over Rad50 (1.05:1 ratio, Mre11/Rad50). The ATP concentration was kept at five times the $K_{m,ATP}$ for each protein. The reactions were started by the sequential addition of the protein and the DNA substrate (containing ATP, when applicable) to a well in a black 96-well microplate. The total volume for each individual well was 100 μl. Samples were excited at 520 nM and polarization data were collected at 560 nM. Data were analyzed and K_d values were determined using SigmaPlot.

Oligomeric Determination of the T4 Mre11-Rad50 Complex—Oligomeric determination was carried out as described previously with the exception that 200 mM NaCl was used in the buffer instead of 50 mM NaCl (18).

RESULTS

Rationale for the L101D Mutation—The T4 homology model generated with the Swiss-model server (33) using the structure of the *Pyrococcus furiosus* Mre11 (Protein Data Bank code 3DSC) indicated that Leu^{101} is the bacteriophage T4 amino acid corresponding to residue Leu^{97} from *P. furiosus,* which when mutated has been shown to disrupt dimerization (34). Although it is possible that the T4 homology model may not be entirely accurate, it is highly likely that the prediction for the core T4 Mre11 structure is correct. To date, the published Mre11 structures from a prokaryote (*Thermotoga maritima*), two eukaryotes (human and *Schizosaccharomyces pombe*) and two archaea (*P. furiosus* and *Methanococcus jannaschii*) all share a very similar core catalytic domain (28, 34–37). The dimeric interface of the prokaryotic and archaea Mre11 structures vary somewhat with respect to the orientation of the monomeric subunits, but the residues that make up the hydrophobic interface are highly conserved (37). The equivalent residue in *S. pombe* Mre11 (Ile^{148}) is part of the hydrophobic interface as well (35). However, the human Mre11 dimer interface is somewhat different, with the equivalent residue (Leu^{143}) being part of the interface helix but not spanning the interface. Instead, it may be involved in an interaction with an adjacent helix in the same subunit (36). Despite these differences, we can conclude with some degree of confidence that Leu^{101} resides in or at least very near the bacteriophage T4 Mre11 dimeric interface. We expected that introduction of a negatively charged side chain into this interface would destabilize this region and therefore test the role of this interface in the overall functioning of the MR complex.

TABLE 2

Dissociation constants for dsDNA and ssDNA

Polarization assays were performed in 50 mM Tris-HCl, 50 mM KCl, 0.1 mg/ml BSA, pH 7.6, in the presence of 5 mM $MgCl_2$ at room temperature. Protein concentrations ranged from 0 to 12 μM in each reaction with a DNA concentration of 10 nM. Assays containing ATP had concentrations of 0.25 and 0.185 mM for WT and L101D, respectively. Values were determined by fitting data to simple equilibrium binding mechanism using SigmaPlot software.

Protein	$K_d$dsDNA	K_d ssDNA
	μM	μM
Rad50	0.14 ± 0.01	0.16 ± 0.02
Rad50/ATP	0.22 ± 0.02	0.26 ± 0.02
Mre11	Not detectable	Not detectable
$Mre11_{L101D}$	Not detectable	Not detectable
Mre11/Rad50	0.69 ± 0.09	0.62 ± 0.12
Mre11/Rad50/ATP	0.15 ± 0.03	0.48 ± 0.09
$Mre11_{L101D}$/Rad50	0.62 ± 0.13	0.96 ± 0.13
$Mre11_{L101D}$/Rad50/ATP	0.13 ± 0.03	0.39 ± 0.08

Steady State ATP Hydrolysis Activity—The addition of WT-Mre11 and dsDNA to Rad50 results in a 22-fold increase in $k_{cat,\ ATP}$, a 3-fold increase in $K_{m,\ ATP}$, and an ATP cooperativity increase (*i.e.* Hill coefficient) from 1.4 to 2.4 (18). These parameters were determined for the L101D-MR complex to determine the effect of disrupting the dimeric interface on the allosteric activation of Rad50 (Table 1). The $k_{cat,\ ATP}$ of the L101D-MR-DNA complex was 10-fold lower than that of the WT-MR-DNA complex, whereas the $K_{m,\ ATP}$ and ATP cooperativity was effectively unchanged. In the absence of dsDNA, the $k_{cat,\ ATP}$ of the L101D-MR complex was nearly normal, indicating that the binding of L101D-Mre11 to Rad50 does not negatively affect the conformation of Rad50 in the absence of dsDNA. Consistent with this, the CD spectrum of L101D-Mre11 was essentially identical to that of the WT enzyme (supplemental Fig. S1).

DNA Binding—To determine the relative affinities of WT- and L101D-MR complexes for dsDNA and ssDNA, we employed a fluorescent polarization assay using either dsDNA or ssDNA with a single 5′-hexachlorofluorescein label. As seen in Table 2, Rad50 binds dsDNA with relatively high affinity and is unaffected by the presence of ATP (K_d values of 0.14 and 0.22 μM in the absence and presence of ATP, respectively). Neither WT- nor L101D-Mre11 displays measurable dsDNA binding at concentrations up to 12 μM. Surprisingly, when either WT- or L101D-Mre11 was added to Rad50 in the absence of ATP, the resulting MR complex had weaker affinity for both dsDNA and ssDNA as compared with Rad50 alone (K_d values of 0.69 and 0.62 μM for the WT- and L101D-MR complex, respectively). However, upon addition of ATP, tight binding is restored (K_d values of 0.15 and 0.13 μM for the WT- and L101D-MR complex, respectively). The affinity of Rad50 for ssDNA is nearly

TABLE 3
Oligomeric determination of the WT and L101D-Mre11 and Mre11-Rad50 complex

Analysis was performed using the Sedphat software. Global fits were accomplished with the Simplex fitting algorithm. Molecular mass estimates were derived from a Monte-Carlo simulation for nonlinear analysis. The mass values reported are the average of the derived estimates of three protein concentrations. Errors are the standard deviations of the derived estimates of the three protein concentrations.

Protein	Molecular mass
	Da
WT-Mre11[a]	41,463 ± 769
L101D-Mre11[a]	40,904 ± 1,679
WT-Mre11/WT-Rad50[b]	204,717 ± 7,878
L101D-Mre11/WT-Rad50[b]	227,706 ± 8,614

[a] Deduced molecular mass for Mre11 is 39,168 Da.
[b] Deduced molecular mass for the $Mre11_2$-$Rad50_2$ complex is 205,568 Da.

identical to that of dsDNA (K_d values of 0.16 and 0.26 μM in the absence and presence of ATP, respectively). Also, similar to what was observed with dsDNA, both the WT- and L101D-MR complex have lower affinity for ssDNA as compared with Rad50 alone (K_d values of 0.62 and 0.96 μM for the WT- and L101D-MR complex, respectively). However, unlike dsDNA binding, the inclusion of ATP does not greatly affect the affinity of the MR complex for ssDNA (K_d values of 0.48 and 0.39 μM for the WT- and L101D-MR complex, respectively).

Competition by L101D-Mre11 with WT-Mre11 for Rad50—To compare the affinity of WT-Mre11 and L101D-Mre11 for Rad50 a spectrophotometric ATPase assay was utilized. In the assay, WT-Mre11 and Rad50 were both held at a concentration of 0.1 μM, and DNA was saturating at 1 μM. The concentration of L101D-Mre11 was varied between 0 and 1.0 μM. The relatively low $k_{cat,\ ATP}$ of the L101D-MR complex compared with the WT-MR complex made this a suitable assay (*i.e.* formation of the L101D-MR complex will result in a lower activity compared with the WT-MR complex). The apparent $k_{cat,\ ATP}$ (*i.e.* a specific activity determination at saturating concentrations of ATP and DNA) was determined and plotted for each condition (Fig. 2*B*). As seen in Fig. 2*B*, L101D-Mre11 successfully outcompeted WT-Mre11, with a calculated IC_{50} of 0.11 ± 0.01 μM, which indicates equal affinity because the concentration of WT-Mre11 was 0.1 μM.

Oligomeric Determination of the T4 Mre11-Rad50 Complex—We previously determined that the T4 WT-MR complex is a heterotetramer ($Mre11_2$/$Rad50_2$) in solution using sedimentation equilibrium analytical ultracentrifugation (AUC) (31). Here, we again used AUC to determine the oligomeric state of WT-Mre11, L101D-Mre11, and the L101D-MR complex. Because of the instability of Rad50 alone during the prolonged AUC run (~96 h), we were unfortunately unable to determine its oligomeric state in the absence of bound Mre11. The determined molecular weights are provided in Table 3. We found that both WT- and L101D-Mre11 proteins are monomeric in the absence of Rad50 (41.4 and 40.9 kDa, respectively, with a calculated mass for the monomer of 39.1 kDa). As suggested by the competition assay, L101D-Mre11 forms a stable complex with Rad50 and has the expected molecular mass for a $Mre11_2$/$Rad50_2$ heterotetramer of 227.7 kDa (supplemental Fig. S2), with a calculated mass for the heterotetramer of 205.6 kDa. A model containing an equilibrium between MR complex tetramers and dimeric and/or monomeric subunits was not required to produce small residuals.

Nuclease Activity—The ssDNA endonuclease activity was probed using a circular M13 substrate. As shown in Fig. 2*C*, under these conditions neither WT-Mre11 nor L101D-Mre11 alone is effective as an ssDNA endonuclease. However, in the presence of Rad50, even in the absence of ATP, the endonuclease activity of both the WT- and L101D-MR complex is apparent. The Rad50-induced enhancement of endonuclease activity is another indication that the L101D mutation does not affect the ability of Mre11 to bind to Rad50. Additionally, the mutation does not appear to have a significant impact on the ssDNA endonuclease of the complex, consistent with results from the *P. furiosus* system (34).

The exonuclease activity of the WT and L101D-MR complexes were first investigated using a uniformly P-32 labeled 1.96-kb linear blunt-ended DNA substrate. Nuclease activity was detected by separating the substrate and products using TLC, visualized by exposure to a PhosphorImager plate, and quantified using ImageJ (Fig. 2*D*). The WT-MR complex exonuclease activity was fit to Equation 1 with single exponential and linear terms,

$$y = a(1 - e^{-bx}) + (cx + d) \quad \text{(Eq. 1)}$$

The single exponential represents the dsDNA exonuclease activity, and the much slower linear phase presumably represents an ssDNA nuclease reaction. The analysis provided a rate of 9.9 ± 1.2 nts removed per s. Because the slow linear phase was less apparent compared with the WT reaction (likely due to the slower exponential phase), the data for the L101D-MR complex were fit to a simple single exponential Equation 2,

$$y = a(1 - e^{-bx}) \quad \text{(Eq. 2)}$$

The determined rate constant for the L101D-MR complex was 1.1 ± 0.1 nts removed per s.

The steady state nuclease activity was then assayed using a denaturing polyacrylamide gel to visualize the product profile of a 50-bp hexachlorofluorescein-labeled DNA substrate (Fig. 3*A*). The ATP-dependent activity produces short DNA products (*i.e.* less than 10 nts) at the early time points, indicating that the WT-MR complex is reasonably processive. The L101D-MR complex does not appear to have the same level as processivity. It does, however, appear to be more efficient at initiating the nuclease reaction compared with the WT-MR complex, as judged by the more rapid loss of the 50-bp DNA substrate. We also monitored the steady state exonuclease activity of the WT- and L101D-MR complex using a real time fluorescent assay using 2-AP as a reporter for nucleotide removal. Liberation of the 2-AP from the dsDNA substrate results in a large increase in fluorescence at 375 nm. We placed 2-AP probes at various positions along the DNA substrate and followed their removal at saturating concentrations of ATP. As seen in Fig. 3*B*, the L101D-MR complex outperforms the WT-MR complex at each 2-AP position by a range of 2–22-fold, consistent with the PAGE analysis.

In contrast to the ATP-dependent exonuclease reaction, in the absence of ATP, the L101D-MR complex has lower activity

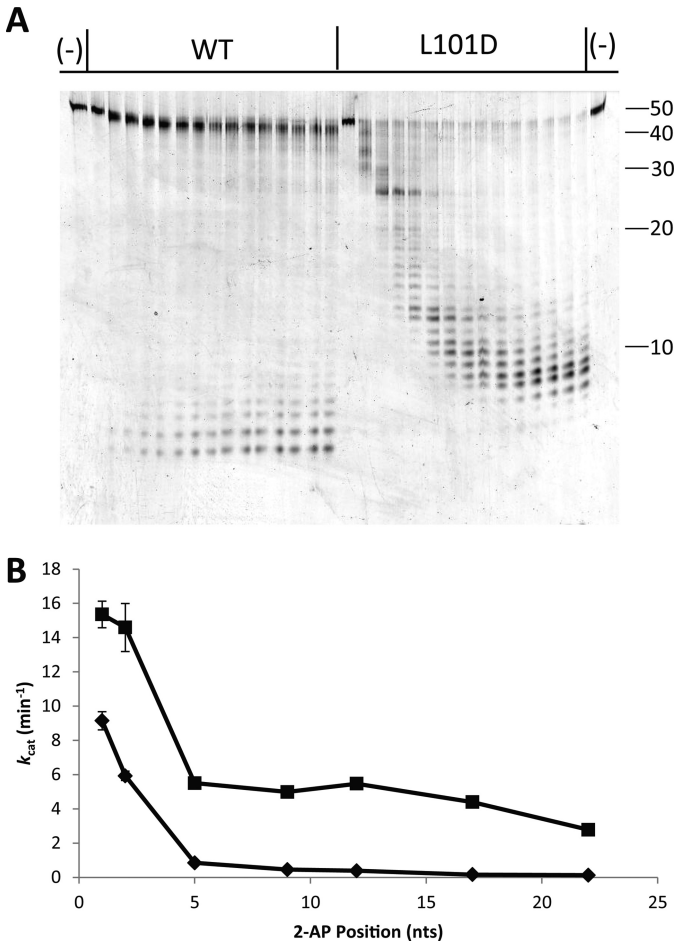

FIGURE 3. **Steady state exonuclease activity in the presence of ATP.** *A,* visualization of nuclease products on a 16% urea-polyacrylamide gel is shown. Each assay consisted of the standard buffer with 0.3 mM $MnCl_2$, 100 nM Rad50, 105 nM Mre11, and 1.3 μM DNA substrate. Time points for each protein are 0, 5, 10, 15, 20, 30, 40, 50, 60, 70, 80, 90, 100, 110, and 120 min. The *1st* and *last lanes* are no protein controls. Approximate mobility of various DNA lengths is shown on the *right-hand side* of the gel. *B,* plot of the k_{cat} exonuclease for either the WT-MR complex (*closed diamonds*) or the L101D-MR complex (*closed squares*) with the 2-AP probe at various positions along the DNA substrate relative to the 3′ end. Protein, DNA, and ATP concentrations are given under "Experimental Procedures."

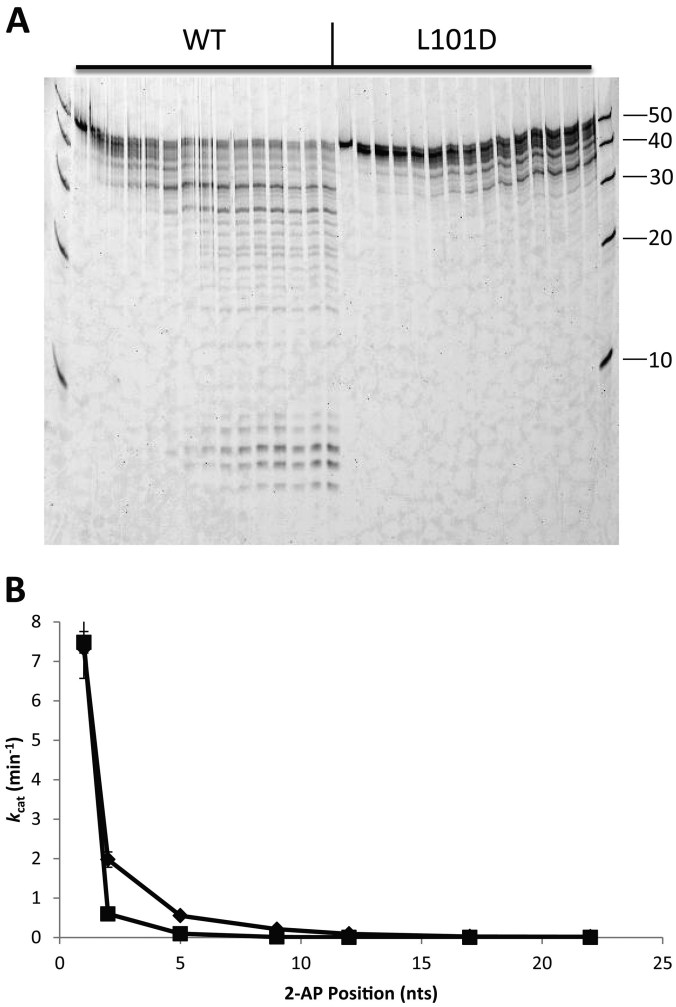

FIGURE 4. **Steady state exonuclease activity in the absence of ATP.** *A,* visualization of nuclease products on a 16% urea-polyacrylamide gel is shown. Each assay consisted of the standard buffer with 0.3 mM $MnCl_2$, 200 nM Rad50, 210 nM Mre11, and 1.3 μM DNA substrate. Time points for each protein are 0, 5, 10, 15, 20, 30, 40, 50, 60, 70, 80, 90, 100, 110, and 120 min. The *1st* and *last lanes* are DNA standards with lengths of 50, 40 30, 20, and 10 nts. *B,* plot of the k_{cat} exonuclease for either the WT-MR complex (*closed diamonds*) or the L101D-MR complex (*closed squares*) with the 2-AP probe at various positions along the DNA substrate relative to the 3′ end. Protein, DNA, and ATP concentrations are given under "Experimental Procedures."

compared with the WT-MR complex. PAGE analysis of the nuclease reaction (Fig. 4) indicates that although the L101D-MR complex appears to initiate the nuclease reaction normally (a single cut is seen at the first time point), it is very slow to make subsequent nucleotide excisions. The ATP-independent exonuclease reaction carried out by the WT-MR complex appears less processive than in the presence of ATP, but DNA products of less than 10 nts in length are still observed starting at approximately the 50-min time point. The 2-AP fluorescence assay (Fig. 4*B*) is consistent with the PAGE analysis; when the 2-AP probe is at the 1st position the WT- and L101D-MR complexes have nearly identical exonuclease rates. However, when the 2-AP probe is moved away from the 3′ end, the exonuclease activity of the WT-MR complex exceeds that of the L101D-MR complex.

We next examined the pre-steady state exonuclease activity of the WT- and L101D-MR complex. The product profile of the ATP-dependent reaction was visualized using denaturing PAGE. In the pre-steady state reaction, the concentration of protein is held in a 30-fold excess over the concentration of DNA substrate. As shown in Fig. 5, similar patterns are seen in the pre-steady state product profile as were seen in the steady state assay (Fig. 3*A*). The WT-MR complex produces products of the final length (distributed around 5 nts) even at the earliest time point. Because no intermediate lengths of product DNA are observed, we tested the possibility that the products are the result of an endonuclease activity cutting approximately ~5 bp from the 5′ ^{32}P label instead of the expected 3′- to 5′-exonuclease activity. We performed a reaction under identical conditions but used a DNA substrate containing a phosphorothioate linkage 24 nts away from the 3′ end. As seen in Fig. 5*B*, a build up of products is seen at the exact position of the phosphorothioate linkage, indicating that the products produced in Fig. 5*A* are the result of exonuclease activity. The pre-steady state product profile of the L101D-MR complex reaction mirrors

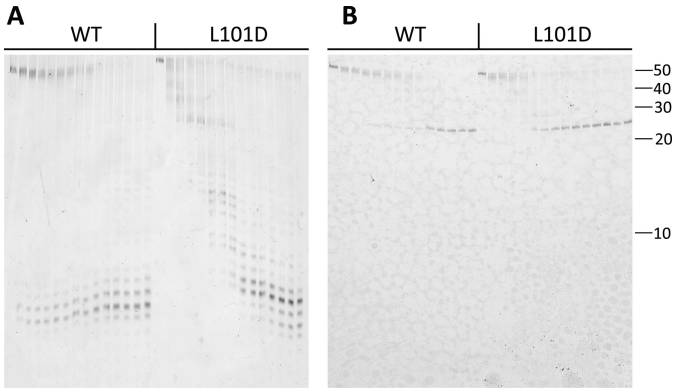

FIGURE 5. **Pre-steady state exonuclease activity in presence of ATP visualized with urea-PAGE.** *A,* assay using standard 50-bp substrate with biotin/streptavidin blocking the 3′ end of ds50-R. Each assay consisted of the standard buffer with 0.3 mM $MnCl_2$, 3 μM Rad50, 3.15 μM Mre11, and 100 nM DNA substrate. Time points for each protein are 0, 3, 5, 7, 10, 15, 20, 25, 30, 40, 50, 60, 80, 100, and 120 s. *B,* assay using 50-bp substrate with biotin/streptavidin blocking the 3′ end of ds50-R and a phosphorothioate linkage at position 26 on ds50-F. The conditions and time points were identical to those in *A,* except that the 40-s time point was omitted from WT-MR complex reaction.

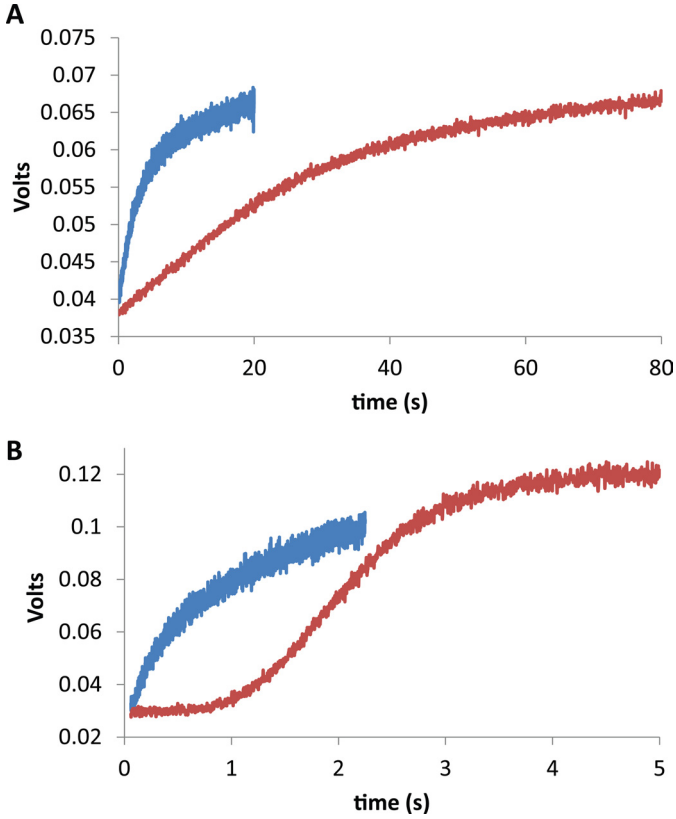

FIGURE 6. **Pre-steady state exonuclease activity in presence of ATP monitored using stopped-flow fluorescence and 2-AP containing DNA substrates.** The assays were carried out at 30 °C in the standard buffer with 0.3 mM $MnCl_2$. The *blue* and *red traces* are the exonuclease activity using the 50-bp DNA substrate with the 2-AP probe located at the 1st and 12th positions, respectively, relative to the 3′ end of the DNA. *A,* exonuclease activity of the WT-MR complex. Each assay consisted of 1 mM ATP, 200 nM DNA, and 3 μM WT-MR complex. *B,* exonuclease activity of the L101D-MR complex. Each assay consisted of 1 mM ATP, 200 nM DNA, and 2 μM L101D-MR complex.

that of the steady state reaction. In contrast to the WT-MR complex, intermediate lengths of DNA are observed between the full-length DNA substrate and the final product. The smallest product in the L101D reaction does not appear until approximately the 30-s time point, and a progressive decrease in product length was observed with increasing time.

We also employed the 2-AP probe to monitor the ATP-dependent pre-steady state exonuclease activity of the WT- and L101D-MR complexes in using stopped-flow fluorescence. The 2-AP probe was placed at either the 1st or 12th nucleotide relative to the 3′ end of the DNA substrate. As seen in Fig. 6, the results mirror that of the pre-steady state reactions analyzed using denaturing PAGE. The WT-MR complex is significantly slower than the L101D-MR complex at removing the 2-AP probe located at either the 1st or 12th position (Fig. 6, *A* and *B*, *blue traces*); however, the WT-MR complex product curve using the 12th position DNA substrate displays no lag period (Fig. 6*A*, *red trace*), whereas a prominent lag is observed in the L101D-MR complex reaction (Fig. 6*B*, *red trace*).

DISCUSSION

It is thought that the Rad50 and Mre11 subunits of the MR complex are allosterically coupled to each other (24, 25, 27, 28, 38). X-ray crystal structures and protein-protein cross-linking experiments have demonstrated that ATP binding and/or hydrolysis by Rad50 affects the conformation of Mre11 (25, 27). Our data have shown that the communication between Rad50 and Mre11 is bidirectional, with Mre11 affecting the catalytic activity of Rad50 (18). WT-Mre11, along with dsDNA, increases the ATP hydrolysis activity of T4 Rad50 by ~20-fold (18). A similar degree of activation (20-fold) is observed with nuclease-deficient Mre11 mutants, indicating that the activation is not directly related to the nuclease activity of Mre11.[3] However, this allosteric activation by DNA may not be general to MR complexes from all species. The ATPase activity of the MR complex from *P. furiosus* is unaffected by addition of dsDNA (39), although it is unclear if the lack of activation is due to the absence of a zinc-hook in the mutant Rad50 protein that was used. We have found that in the T4 system, site-directed mutation of the zinc-hook completely eliminates the DNA activation of the ATPase activity.[4] In contrast to WT-Mre11, L101D-Mre11 only activates Rad50 ATP hydrolysis 2-fold in the presence of dsDNA. This decrease in activation is not due to a decrease in the stability of the complex because nuclease, Rad50 competition, and AUC experiments all indicate that the affinity of L101D-Mre11 for Rad50 is unaffected by the mutation. DNA binding experiments also indicate that the L101D-MR complex has normal affinity toward dsDNA.

The decrease in DNA activation of the L101D-MR complex suggests that when DNA is present, there is a tight coupling between the altered structure of the Mre11 dimer interface and the structure/activity of Rad50. However, the ATPase activity of the L101D-MR complex is nearly normal without DNA, suggesting that the tight coupling between Mre11 and Rad50 requires the formation of the MR-DNA complex. Alternatively, it is possible that the Mre11 dimer interface only forms in the presence of dsDNA so that the introduction of the L101D mutation has no effect on the conformation of Mre11 in the

[3] D. W. Albrecht and S. W. Nelson, unpublished observations.

[4] T. C. Barfoot and S. W. Nelson, unpublished observations.

absence of DNA. However, the available crystal structures of the MR complex argue against this possibility because they have all shown a dimeric Mre11, regardless of the presence or absence of a bound DNA substrate (25, 28, 34, 36, 37).

The ATP-independent nuclease activity of L101D-Mre11 on ssDNA (Fig. 2*C*) and dsDNA with the 2-AP probe at the 1st position (Fig. 4*B*) demonstrates that the intrinsic nuclease activity of L101D-Mre11 is unaffected. This indicates that the Mre11 active site is unperturbed, suggesting that the conformation of the L101D-Mre11 subunit itself is not greatly affected by the introduction of the negative charge into the dimer interface. However, the ATP-dependent exonuclease activity of the L101D-MR complex, when assayed using a 1.96-kb dsDNA substrate, is reduced by 9.2-fold (Fig. 2*D*). Because the intrinsic nuclease rate of L101D-Mre11 appears to be normal, the reduction in repetitive exonuclease activity is likely caused by a reduction in processivity or the translocation rate, which may be linked to the reduced ATP hydrolysis of the L101D-MR-DNA complex.

Based on the decrease in exonuclease activity of the L101D-MR complex when assayed with the 1.96-kb DNA substrate, we were surprised to observe elevated nuclease rates when assayed with the 50-bp dsDNA substrate. In the presence of ATP, the L101D-MR complex displays higher activity than the WT-MR complex when the 2-AP nuclease probe is placed at positions ranging from 1 to 22 (Fig. 3*B*). We have previously determined the rate-limiting step of the steady state nuclease reaction to be the productive assembly of the MR complex onto the DNA substrate (31, 38). Therefore, the higher activity of the L101D-MR complex suggests that its productive assembly rate is increased compared with the WT-MR complex. We are using the term "productive assembly" to represent an event that differs from simple DNA binding. Our DNA binding assays indicate that the L101D-MR complex has nearly identical affinity for duplex DNA as the WT-MR complex. Additionally, a comparison of the ATP hydrolysis to the exonuclease rates suggests that the WT-MR complex likely undergoes several rounds of unproductive binding events prior to successfully removing the first nucleotide from the DNA substrate (the k_{cat} values for ATP hydrolysis and 1st nucleotide removal are 3.2 and 0.15 s^{-1}, respectively).

The PAGE analysis of a 5′-labeled DNA substrate is consistent with a faster assembly rate and also reveals that the processivity of the L101D-MR is greatly reduced compared with the WT-MR complex (Fig. 3*A*). In the WT-MR complex reaction, very few intermediates are observed between the full-length DNA substrate and the final products that are less than 10 nts in length. This pattern is highly indicative of a slow rate-limiting assembly step, followed by a rapid (relative to the acquisition time) and processive exonuclease reaction. However, in the case of the L101D-MR complex, the pattern is more indicative of rapid assembly and a rate-liming nucleotide excision or translocation step (Fig. 3*B*). Because the intrinsic nuclease activity of the L101D-MR complex is unaffected, it suggests that the defect lies in the translocation step that follows nucleotide excision. Also, the L101D-MR complex does not excise as many nucleotides from the DNA substrate as the WT enzyme (*i.e.* the smallest product for WT is ~3 nts, whereas for L101D it is ~6 nts). The cause of this difference is not clear, but it is possible that the size of the DNA remaining is simply related to the melting temperature of the DNA strand and the speed at which the MR complex moves along the DNA substrate (*i.e.* the WT complex excises more nucleotides prior to DNA strand melting due to its higher processivity and speed of translocation). This explanation is consistent with the production of a range of products rather than a single discrete band.

The more rapid assembly of the L101D-MR complex as compared with the WT complex is difficult to explain within the context of an Mre11 dimer interface that is stable and unchanging throughout the nuclease reaction cycle. The x-ray crystal structures of the truncated MR complex in the absence and presence of ATP suggest minor changes in the Mre11 dimer interface, and biochemical experiments suggest a dynamic interface as well (25, 27). Protein cross-linking experiments performed by Hopfner and co-workers (27) indicate that binding of ATP to the MR complex alters the conformation of the Mre11 dimer interface, which causes a decrease in cross-linking efficiency. Inclusion of ADP rather than ATP increases cross-linking efficiency, indicating that ATP and ADP stabilize different forms of the Mre11 dimer interface. It is unclear whether the L101D mutation is stabilizing the apo-form, ADP form, or ATP form of the Mre11 dimer interface, or whether it produces an alternative conformation that the WT-MR complex does not normally adopt during its nuclease cycle. It is tempting to speculate, however, that because the L101D-MR complex has a more rapid productive assembly rate and a normal intrinsic nuclease rate, the mutation stabilizes the native conformation of the MR complex that is most competent for initiation of nuclease activity.

The pre-steady state kinetic data are also consistent with a slow rate-limiting assembly of the WT-MR complex, followed by a rapid and processive exonuclease reaction. In the reaction shown in Fig. 5*A*, the ratio of protein to DNA is 30:1, and the reaction rate has reached a protein-independent phase, such that increasing the concentration of protein has no effect on the apparent rate of the reaction. Even at these extremely high protein concentrations, the product pattern is similar to that seen in the steady state nuclease reaction shown in Fig. 3*A*. The absence of observable intermediates (i.e. DNA fragments between 49 and 10 nts) in this reaction indicates that the rate-limiting step remains productive assembly.

The shape of the product formation curve in the pre-steady state stopped-flow experiments (Fig. 6, *A* and *B*) also provides information regarding the rate-limiting steps of the nuclease reaction. In the situation where productive assembly is fast compared with the translocation/nuclease rate, a distinct lag phase should be seen as the probe is moved away from the 1st position, analogous to what is often observed in all-or-none helicase unwinding assays (40). This is precisely what is observed in the L101D-MR complex reaction, consistent with the conclusions from the steady state and pre-steady state PAGE analysis. However, the product formation curve of the WT-MR complex shows no apparent lag as the probe is moved away from the 3′ end of the DNA. Again, as the PAGE analysis suggested, this is consistent with a rate-limiting productive

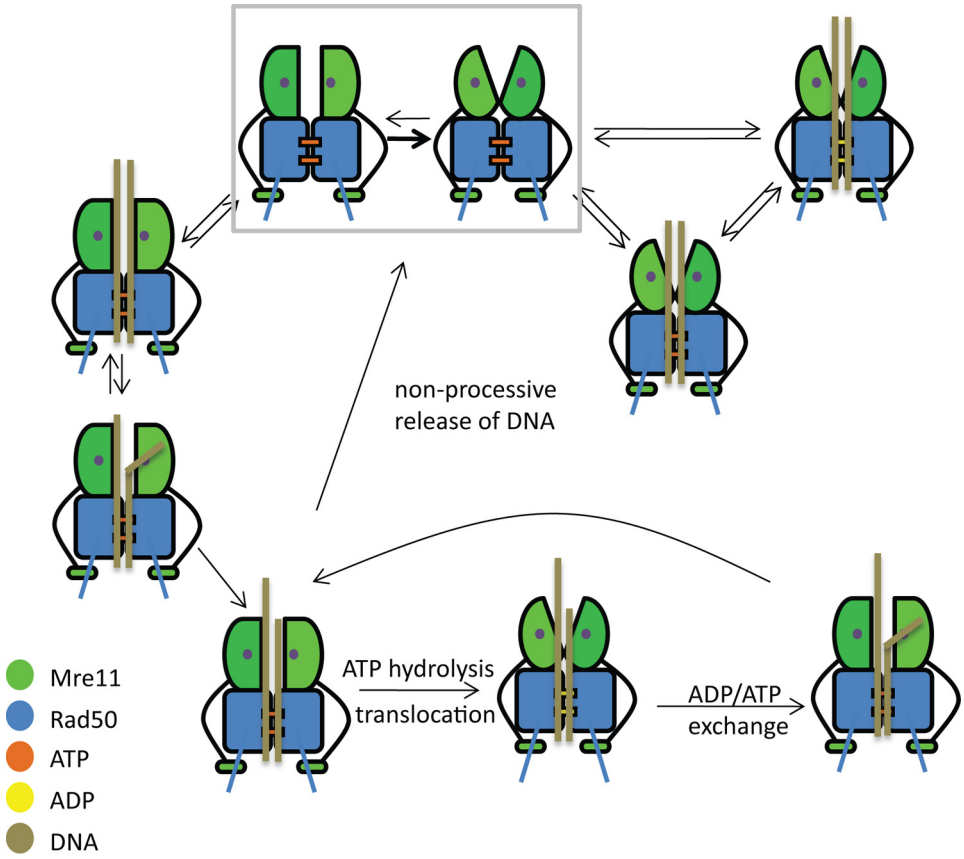

FIGURE 7. **Proposed two-state model for the Mre11 dimer interface based on studies of the T4 MR complex (gp46/47).** Details of the model can be found in the text of the "Discussion." A color legend can be found in the *lower left-hand corner*. The *small purple circle* found on each Mre11 subunit represents the nuclease activity site. The initiation state of the MR complex is depicted as having a parallel Mre11 dimeric interface, and the translocation state is depicted with the Mre11 dimer interface in close contact at one end (*V-shaped*).

assembly step, followed by rapid exonuclease activity and translocation.

Based on the data presented here, we propose a two-state working model for the Mre11 dimer interface (Fig. 7). The first state (the "nuclease initiation state") forms during the initiation of nuclease activity and is promoted by the L101D mutation. The second state (the "translocation state") forms during the processive exonuclease reaction, likely an ATP hydrolysis-driven translocation step, and is hindered by the L101D mutation. The exact nature of the Mre11 dimeric interface in these two states is unknown. Given the extreme nature of the Leu^{101} to Asp mutation, it is tempting to speculate that in the nuclease initiation state, the Mre11 dimeric interface is altered in such a way as to remove the leucine residue from the hydrophobic pocket that is observed in the x-ray crystal structures. We propose that the Mre11 dimeric interface that has been repeatedly observed in the x-ray crystal structures (*i.e.* with Leu^{101} engaged in the hydrophobic pocket) is the conformation of the translocation state.

Our current working model for the Mre11 interface has the WT-MR complex sampling both states when not bound to DNA, with the equilibrium lying in the direction of the translocation state. This equilibrium is included in the model to explain the observation that the DNA-dependent ATP hydrolysis rate is much faster than the steady state nuclease rate (*i.e.* all binding events result in ATP hydrolysis, but only a few result in the excision of a nucleotide from the DNA substrate). Following productive assembly, the MR complex remains in the "initiation state" for the removal of the nucleotide from the 3′ end of the dsDNA. If nucleotide excision occurs in the absence of ATP, a portion of the WT-MR complex dissociates from the DNA, where it can rebind DNA substrate to excise another nucleotide (nonprocessive translocation). The release of the DNA by the MR complex may involve a conformational change in the Mre11 dimer interface, because the L101D-MR complex appears to stall on the DNA substrate in the absence of ATP, rather than releasing it at the same rate at the WT-MR complex (see Fig. 4). After nucleotide excision in the presence of ATP, ATP hydrolysis by the WT-MR complex triggers a conformational change to the translocation state, and the complex translocates along the nascent ssDNA in preparation for the next nucleotide excision. The translocation step itself could occur following either ATP hydrolysis or ADP/P_i product release. After the translocation step, the WT-MR complex returns to the nuclease initiation state to complete the cycle. The L101D-MR complex binds and hydrolyzes ATP (albeit at a slower rate than WT), but because it is unable to form the translocation state, it dissociates from the DNA rather than moving forward for the next nucleotide removal, hence its lower processivity.

As suggested previously by Hopfner and co-workers (27), a model involving repetitive conformational changes in Mre11, which are driven by Rad50 ATP hydrolysis, is reminiscent of how the NBD of ABC transporters drive the opening and closing of their transmembrane domain to allow substrates into or

out of the cell (16). This is consistent with the notion that all members of the ABC protein superfamily share a unified functional architecture (19, 27).

REFERENCES

1. Povirk, L. F. (2006) Biochemical mechanisms of chromosomal translocations resulting from DNA double strand breaks. *DNA Repair* **5,** 1199–1212
2. Bassing, C. H., and Alt, F. W. (2004) The cellular response to general and programmed DNA double strand breaks. *DNA Repair* **3,** 781–796
3. McVey, M., and Lee, S. E. (2008) MMEJ repair of double strand breaks (director's cut). Deleted sequences and alternative endings. *Trends Genet.* **24,** 529–538
4. Connelly, J. C., and Leach, D. R. (2002) Tethering on the brink. The evolutionarily conserved Mre11-Rad50 complex. *Trends Biochem. Sci.* **27,** 410–418
5. San Filippo, J., Sung, P., and Klein, H. (2008) Mechanism of eukaryotic homologous recombination. *Annu. Rev. Biochem.* **77,** 229–257
6. Mimitou, E. P., and Symington, L. S. (2008) Sae2, Exo1, and Sgs1 collaborate in DNA double strand break processing. *Nature* **455,** 770–774
7. Cejka, P., Cannavo, E., Polaczek, P., Masuda-Sasa, T., Pokharel, S., Campbell, J. L., and Kowalczykowski, S. C. (2010) DNA end resection by Dna2-Sgs1-RPA and its stimulation by Top3-Rmi1 and Mre11-Rad50-Xrs2. *Nature* **467,** 112–116
8. Zhu, Z., Chung, W. H., Shim, E. Y., Lee, S. E., and Ira, G. (2008) Sgs1 helicase and two nucleases Dna2 and Exo1 resect DNA double strand break ends. *Cell* **134,** 981–994
9. Symington, L. S. (2002) Role of RAD52 epistasis group genes in homologous recombination and double strand break repair. *Microbiol. Mol. Biol. Rev.* **66,** 630–670
10. Krogh, B. O., and Symington, L. S. (2004) Recombination proteins in yeast. *Annu. Rev. Genet.* **38,** 233–271
11. Dillingham, M. S., and Kowalczykowski, S. C. (2008) RecBCD enzyme and the repair of double-stranded DNA breaks. *Microbiol. Mol. Biol. Rev.* **72,** 642–671
12. Kreuzer, K. N., Yap, W. Y., Menkens, A. E., and Engman, H. W. (1988) Recombination-dependent replication of plasmids during bacteriophage T4 infection. *J. Biol. Chem.* **263,** 11366–11373
13. Mosig, G. (1998) Recombination and recombination-dependent DNA replication in bacteriophage T4. *Annu. Rev. Genet.* **32,** 379–413
14. Nossal, N. G. (1992) Protein-protein interactions at a DNA replication fork. Bacteriophage T4 as a model. *FASEB J.* **6,** 871–878
15. Hopfner, K. (2003) Rad50/SMC proteins and ABC transporters. Unifying concepts from high resolution structures. *Curr. Opin. Struct. Biol.* **13,** 249–255
16. Jones, P. M., O'Mara, M. L., and George, A. M. (2009) ABC transporters. A riddle wrapped in a mystery inside an enigma. *Trends Biochem. Sci.* **34,** 520–531
17. Davidson, A. L., Dassa, E., Orelle, C., and Chen, J. (2008) Structure, function, and evolution of bacterial ATP-binding cassette systems. *Microbiol. Mol. Biol. Rev.* **72,** 317–364
18. Herdendorf, T. J., Albrecht, D. W., Benkovic, S. J., and Nelson, S. W. (2011) Biochemical characterization of bacteriophage T4 Mre11-Rad50 complex. *J. Biol. Chem.* **286,** 2382–2392
19. Hopfner, K. P., Karcher, A., Shin, D. S., Craig, L., Arthur, L. M., Carney, J. P., and Tainer, J. A. (2000) Structural biology of Rad50 ATPase. ATP-driven conformational control in DNA double strand break repair and the ABC-ATPase superfamily. *Cell* **101,** 789–800
20. Barford, D., Das, A. K., and Egloff, M. P. (1998) The structure and mechanism of protein phosphatases. Insights into catalysis and regulation. *Annu. Rev. Biophys. Biomol. Struct.* **27,** 133–164
21. Bressan, D. A., Baxter, B. K., and Petrini, J. H. (1999) The Mre11-Rad50-Xrs2 protein complex facilitates homologous recombination-based double strand break repair in *Saccharomyces cerevisiae*. *Mol. Cell. Biol.* **19,** 7681–7687
22. Buis, J., Wu, Y., Deng, Y., Leddon, J., Westfield, G., Eckersdorff, M., Sekiguchi, J. M., Chang, S., and Ferguson, D. O. (2008) Mre11 nuclease activity has essential roles in DNA repair and genomic stability distinct from ATM activation. *Cell* **135,** 85–96
23. Taylor, A. M., Groom, A., and Byrd, P. J. (2004) Ataxia telangiectasia-like disorder (ATLD). Its clinical presentation and molecular basis. *DNA Repair* **3,** 1219–1225
24. Wyman, C., Lebbink, J., and Kanaar, R. (2011) Mre11-Rad50 complex crystals suggest molecular calisthenics. *DNA Repair* **10,** 1066–1070
25. Möckel, C., Lammens, K., Schele, A., and Hopfner, K. P. (2012) ATP-driven structural changes of the bacterial Mre11-Rad50 catalytic head complex. *Nucleic Acids Res.* **40,** 914–927
26. Williams, G. J., Williams, R. S., Williams, J. S., Moncalian, G., Arvai, A. S., Limbo, O., Guenther, G., SilDas, S., Hammel, M., Russell, P., and Tainer, J. A. (2011) ABC ATPase signature helices in Rad50 link nucleotide state to Mre11 interface for DNA repair. *Nat. Struct. Mol. Biol.* **18,** 423–431
27. Lammens, K., Bemeleit, D. J., Möckel, C., Clausing, E., Schele, A., Hartung, S., Schiller, C. B., Lucas, M., Angermüller, C., Söding, J., Strässer, K., and Hopfner, K. P. (2011) The Mre11:Rad50 structure shows an ATP-dependent molecular clamp in DNA double strand break repair. *Cell* **145,** 54–66
28. Lim, H. S., Kim, J. S., Park, Y. B., Gwon, G. H., and Cho, Y. (2011) Crystal structure of the Mre11-Rad50-ATPγS complex. Understanding the interplay between Mre11 and Rad50. *Genes Dev.* **25,** 1091–1104
29. Hopfner, K. P., Craig, L., Moncalian, G., Zinkel, R. A., Usui, T., Owen, B. A., Karcher, A., Henderson, B., Bodmer, J. L., McMurray, C. T., Carney, J. P., Petrini, J. H., and Tainer, J. A. (2002) The Rad50 zinc-hook is a structure joining Mre11 complexes in DNA recombination and repair. *Nature* **418,** 562–566
30. Moreno-Herrero, F., de Jager, M., Dekker, N. H., Kanaar, R., Wyman, C., and Dekker, C. (2005) Mesoscale conformational changes in the DNA-repair complex Rad50-Mre11-Nbs1 upon binding DNA. *Nature* **437,** 440–443
31. Herdendorf, T. J., and Nelson, S. W. (2011) Functional evaluation of bacteriophage T4 Rad50 signature motif residues. *Biochemistry* **50,** 6030–6040
32. Gilbert, S. P., and Mackey, A. T. (2000) Kinetics. A tool to study molecular motors. *Methods* **22,** 337–354
33. Arnold, K., Bordoli, L., Kopp, J., and Schwede, T. (2006) The SWISS-MODEL workspace. A web-based environment for protein structure homology modeling. *Bioinformatics* **22,** 195–201
34. Williams, R. S., Moncalian, G., Williams, J. S., Yamada, Y., Limbo, O., Shin, D. S., Groocock, L. M., Cahill, D., Hitomi, C., Guenther, G., Moiani, D., Carney, J. P., Russell, P., and Tainer, J. A. (2008) Mre11 dimers coordinate DNA end bridging and nuclease processing in double strand-break repair. *Cell* **135,** 97–109
35. Schiller, C. B., Lammens, K., Guerini, I., Coordes, B., Feldmann, H., Schlauderer, F., Möckel, C., Schele, A., Strässer, K., Jackson, S. P., and Hopfner, K. P. (2012) Structure of Mre11-Nbs1 complex yields insights into ataxia telangiectasia-like disease mutations and DNA damage signaling. *Nat. Struct. Mol. Biol.* **19,** 693–700
36. Park, Y. B., Chae, J., Kim, Y. C., and Cho, Y. (2011) Crystal structure of human Mre11. Understanding tumorigenic mutations. *Structure* **19,** 1591–1602
37. Das, D., Moiani, D., Axelrod, H. L., Miller, M. D., McMullan, D., Jin, K. K., Abdubek, P., Astakhova, T., Burra, P., Carlton, D., Chiu, H. J., Clayton, T., Deller, M. C., Duan, L., Ernst, D., Feuerhelm, J., Grant, J. C., Grzechnik, A., Grzechnik, S. K., Han, G. W., Jaroszewski, L., Klock, H. E., Knuth, M. W., Kozbial, P., Krishna, S. S., Kumar, A., Marciano, D., Morse, A. T., Nigoghossian, E., Okach, L., Paulsen, J., Reyes, R., Rife, C. L., Sefcovic, N., Tien, H. J., Trame, C. B., van den Bedem, H., Weekes, D., Xu, Q., Hodgson, K. O., Wooley, J., Elsliger, M. A., Deacon, A. M., Godzik, A., Lesley, S. A., Tainer, J. A., and Wilson, I. A. (2010) Crystal structure of the first eubacterial Mre11 nuclease reveals novel features that may discriminate substrates during DNA repair. *J. Mol. Biol.* **397,** 647–663
38. De la Rosa, M. B., and Nelson, S. W. (2011) An interaction between the Walker A and D-loop motifs is critical to ATP hydrolysis and cooperativity in bacteriophage T4 Rad50. *J. Biol. Chem.* **286,** 26258–26266
39. Majka, J., Alford, B., Ausio, J., Finn, R. M., and McMurray, C. T. (2012) ATP hydrolysis by RAD50 protein switches MRE11 enzyme from endonuclease to exonuclease. *J. Biol. Chem.* **287,** 2328–2341
40. Lohman, T. M., Tomko, E. J., and Wu, C. G. (2008) Nonhexameric DNA helicases and translocases. Mechanisms and regulation. *Nat. Rev. Mol. Cell Biol.* **9,** 391–401

Figure S1

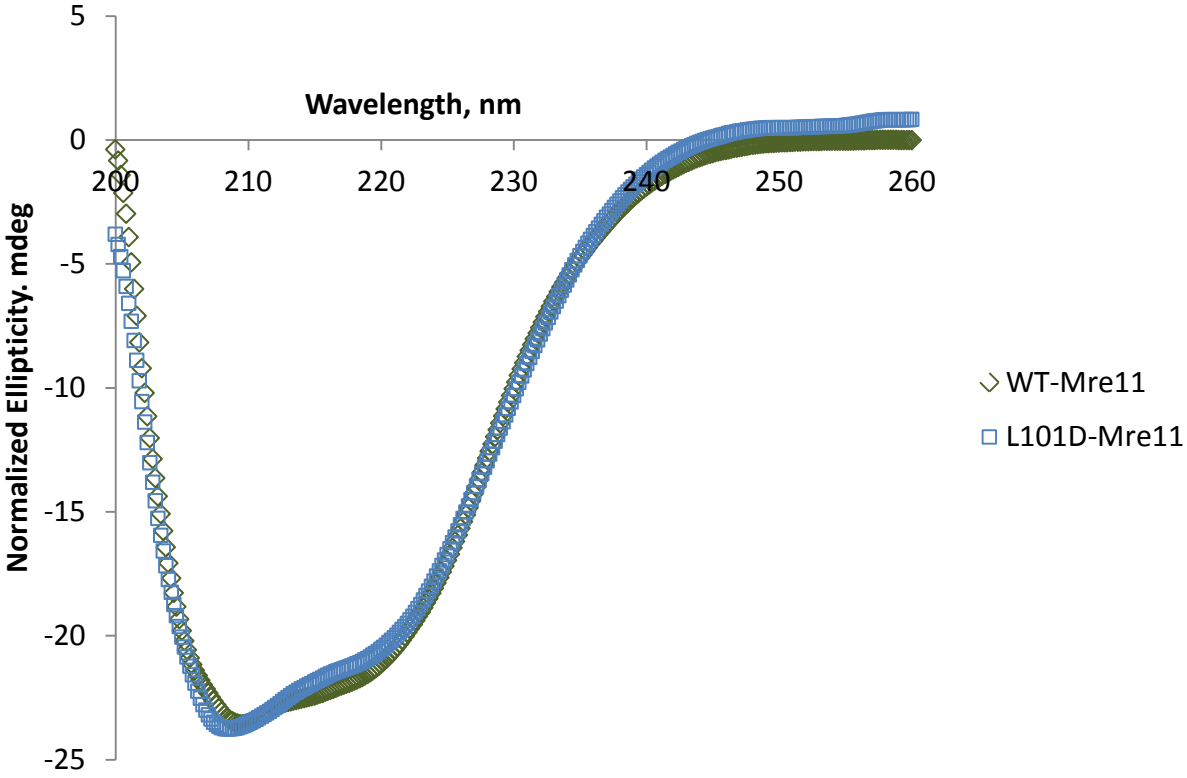

Figure S1. **Circular dichroism spectra of WT- and L101D-Mre11 proteins.** The experiment was carried out as described in "Experimental Procedures".

Figure S2.

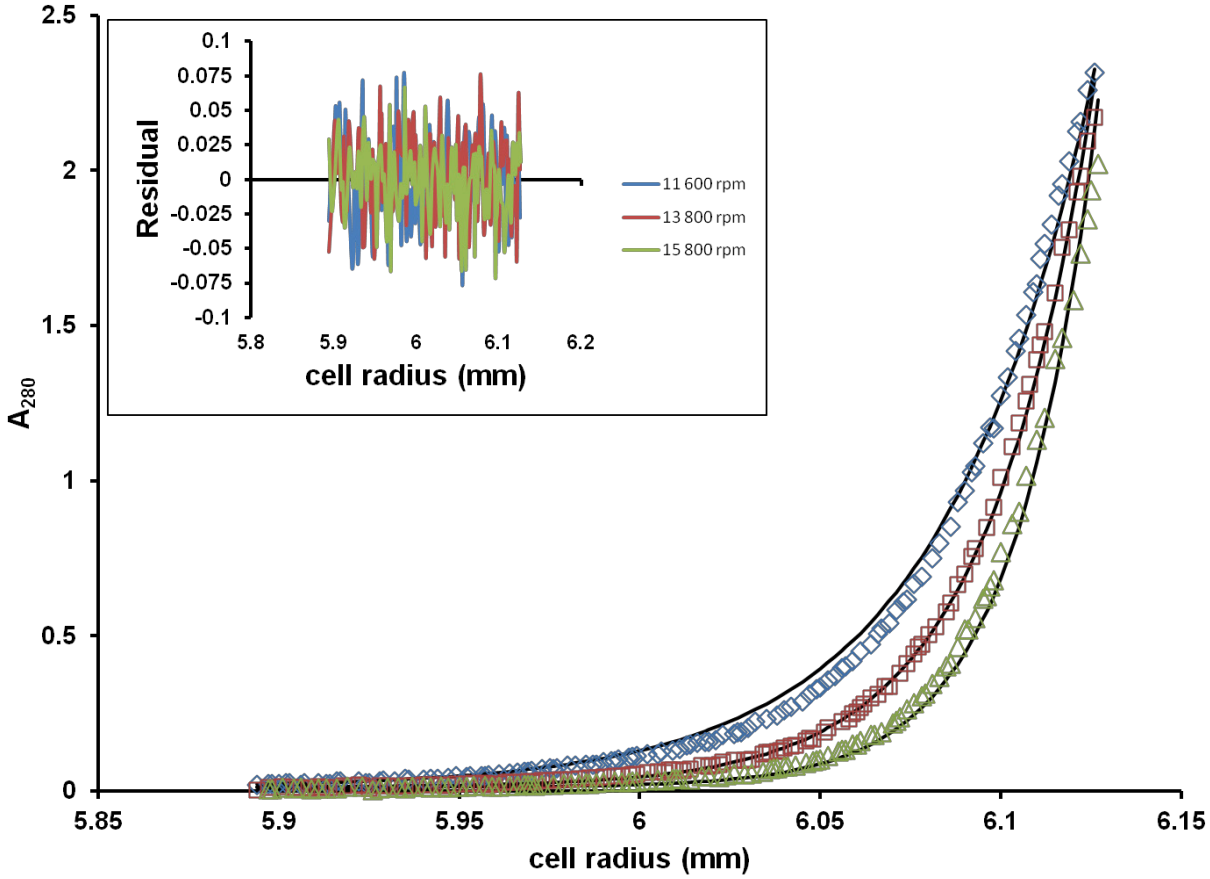

Figure S2. **Oligomeric determination of the WT Rad50/L101D Mre11 complex.** Representative analytical equilibrium ultracentrifugation results for one complex concentration (initial A280: 0.6). Equilibrium concentration gradients were formed at velocities of 11 600 (◊), 13 800 (□), and 15 800 rpm (Δ). Solid lines represent the global fits produced. Inset: fit residuals.

Disruption of the Bacteriophage T4 Mre11 Dimer Interface Reveals a Two-state Mechanism for Exonuclease Activity

Dustin W. Albrecht, Timothy J. Herdendorf and Scott W. Nelson

J. Biol. Chem. 2012, 287:31371-31381.
doi: 10.1074/jbc.M112.392316 originally published online July 13, 2012
